Manufacturing Letters 29 (2021) 29–33

Contents lists available at ScienceDirect

Manufacturing Letters

journal homepage: www.elsevier.com/locate/mfglet

Computational minimization of over-deposition at corners of trajectories in Laser Metal Deposition

Diego Montoya-Zapata [a,b], Carles Creus [a], Aitor Moreno [a,*], Igor Ortiz [c], Piera Alvarez [c], Oscar Ruiz-Salguero [b], Jorge Posada [a]

[a] Vicomtech Foundation, Basque Research and Technology Alliance (BRTA), Mikeletegi 57, Donostia-San Sebastian 20009, Spain
[b] Laboratory of CAD CAM CAE, Universidad EAFIT, Cra 49 no 7-sur-50, Medellín 050022, Colombia
[c] Ikergune A.I.E., San Antolin 3, Elgoibar 20870, Spain

ARTICLE INFO

Article history:
Received 22 March 2021
Accepted 9 May 2021
Available online 24 May 2021

Keywords:
Additive manufacturing
Laser cladding
Optimization

ABSTRACT

Avoidance of over-deposition at trajectory corners is relevant in Laser Metal Deposition (LMD) for Additive Manufacturing. Currently available LMD hardware only allows constant material feed (g/s). Therefore, gliding speed of the material dispenser is the remaining tuning variable for controlling metal over-deposition at corners. Existing literature reports trial–error physical experiments, addressing only particular corner angles. In response, this manuscript reports the implementation of a voxel-based simulator of the bead geometry, taking into consideration bead profile, dispenser velocity, material feed, and bead curve geometry. We use it to evaluate two constant-feed tailored-velocity strategies for minimizing material over-deposition at corners.

1. Introduction

Laser Metal Deposition (LMD) employs a laser beam to melt a jet of metal powder and to deliver it onto a workpiece. This promising Additive Manufacturing (AM) technique is used in workpiece coating, repairing and re-manufacturing [1,2]. However, over-deposition of metal on curved or sharp-corner beads is a standing challenge for LMD.

In this manuscript, we present the implementation of a voxel-based simulator of the bead geometry, taking into consideration bead cross profile, nozzle velocity, variable material feed, and bead curve geometry. Our simulator allows for time-varying material feed (g/s), although this feature is an open research topic at the present time. We couple our bead geometry simulator with two variable speed strategies, used to minimize material over-deposition in corners.

2. Literature review

AM uses Piecewise Linear (PL) trajectories. Two factors reinforce metal over deposition at corners: (i) overlapping deposition zone (Fig. 1(a)) and (ii) nozzle deceleration. The proposed methods in the literature to reduce over-deposition at the corners are (1) the control of the process parameters (e.g. speed, power and material flow) [3], (2) corner smoothing [4–6] and (3) a combination [7,8] of (1) and (2). Corner smoothing is only acceptable if accuracy is not a priority. The authors [3] that aim only to control the process parameters (e.g. speed, power, material flow) do not use numerical methods to study the influence of the parameters in the corner deposition. Instead, they employ costly physical trial–error experimentation and limit their studies to right (90°) angles.

We identified two approaches to model computationally the bead geometry in LMD. The first assumes a pre-defined bead cross-section, namely circular [9–12], elliptical [9,13], parabolic [9,11,12,14,15], sinusoidal [9,11,12]. Other researchers [16,3] model bead width and height as functions of process parameters.

In the second method, the bead geometry is not pre-defined but it is induced by the distribution of the delivered material which depends on the process parameters [17,10,18,19]. We consider that, under conditions of full melting of the powder jet, the variation in nozzle velocity or material feed are more immediate factors to control over-deposition. Mainly two types of delivered material functions have been studied: Gaussian [17,10,18,19] and uniform [10]. Our simulator accepts any material distribution function $f : \mathbb{R}^2 \rightarrow \mathbb{R}$.

* Corresponding author.
E-mail address: amoreno@vicomtech.org (A. Moreno).

https://doi.org/10.1016/j.mfglet.2021.05.001

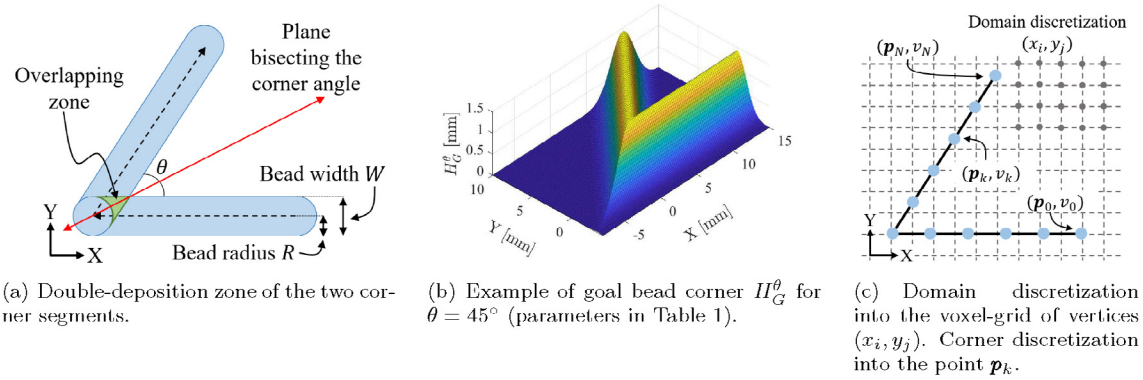

(a) Double-deposition zone of the two corner segments.

(b) Example of goal bead corner H_G^θ for $\theta = 45°$ (parameters in Table 1).

(c) Domain discretization into the voxel-grid of vertices (x_i, y_j). Corner discretization into the point $\boldsymbol{p}_k$.

Fig. 1. Trajectory corner. Parameters, goal bead and discretization.

2.1. Conclusions of the literature review

In the existing literature, sharp corners deposition in LMD is addressed by smoothing the corner geometry and expensive trial-and-error experimentation. This manuscript presents an implementation of a material deposition geometric simulator which considers: bead geometry induced by models of delivered material distribution, PL trajectories, nozzle velocity (mm/s) and feed rate (g/s).

3. Methodology

3.1. Geometry deposition model

3.1.1. Powder delivery density

The function $I(x,y,t)$ (g/(s mm^2)) reflects, given a time t, the metal particle density projected by the nozzle at the workpiece surface. Coordinate z is parallel to the jet. Eq. 1 represents a Gaussian example of this distribution, with coordinates (x,y) already measured on the workpiece surface. Our simulator accepts any density function of (x,y):

$$I(x,y,t) = \frac{2f(t)}{\pi R^2} \exp\left(\frac{-2\left((x-P_x(t))^2 + (y-P_y(t))^2\right)}{R^2}\right). \tag{1}$$

f is the material feed rate (g/s), R is half of the nominal bead width (mm), $\boldsymbol{P}(t) = [P_x(t), P_y(t)]^T$ is the nozzle position (mm, mm) at time t.

Given the function I, the material density ρ and the total deposition time T, one can obtain the bead height H as:

$$H(x,y) = \frac{1}{\rho}\int_0^T I(x,y,\xi)d\xi. \tag{2}$$

3.1.2. Nozzle trajectory

$C = [p0, .., pN]$ is a PL approximation of the nozzle trajectory. f_k and v_k are the feed and velocity levels at point $\boldsymbol{p}_k$. Acceleration is assumed constant when velocity changes. Let $t_k\,(0 \leqslant k \leqslant N)$ be the time at which the dispenser reaches point $\boldsymbol{p}_k$, with $t_0 = 0$ and $t_N = T$. Each t_k is a function of the speeds $v_0, v_1, \ldots, v_k$. We numerically compute the bead height as per Eq. (3):

$$H(x,y) = \frac{1}{\rho}\sum_{k=1}^{N}\int_{t_{k-1}}^{t_k} I(x,y,\xi)d\xi. \tag{3}$$

3.2. Minimization of material overfill in corners

We define an *ideal* corner as the one in which incoming and outgoing beads are free from over- and under-deposition. The ideal bead profile H_0 in Eq. (4) corresponds to the steady state in a linear nozzle trajectory. For the purpose of computing H_0, we may consider this trajectory on the X axis and therefore $H_0(x,y) = H_0(y)$.

$$H_0(x,y) = \int_{-\infty}^{\infty} I(x,y,t)dt = \frac{\sqrt{2}f}{\rho\sqrt{\pi}Rv}\exp\left(\frac{-2y^2}{R^2}\right). \tag{4}$$

The ideal or *goal* corner corresponds to an assembly of incoming and outgoing beads. They are completely symmetrical w.r.t. a plane bisecting the corner angle (Fig. 1).

Considerations for corners in LMD are: (a) Over-deposition is reinforced by (i) overlapping zones in incoming and outgoing beads (Fig. 1), ii) mandatory deceleration to reach null velocity at the corner itself. (b) Current LMD hardware is unable to produce variable feed (g/s) within the trajectory [20,21,3], leading to an overall constant feed. Because of these considerations, we proceed to use the nozzle cruise velocity as variable to minimize material over-deposition at corners.

The tuning variables for the over-deposition minimization are the nozzle speeds $V = (v_0, \ldots, v_N)$ at each vertex $\boldsymbol{p}_k$ of the corner discretization. We define the optimization problem assuming the domain is discretized into a rectangular grid G with vertices $(x_i, y_j), (1 \leqslant i \leqslant G_1, 1 \leqslant j \leqslant G_2)$, as shown in Fig. 1(c). The optimization problem is stated as follows:

$$\begin{aligned} &\text{find} && V = (v_0, \ldots, v_N) \\ &\text{to minimize} && E_k(V) = \tfrac{1}{G_1 G_2}\sum_{i=1}^{G_1}\sum_{j=1}^{G_2} e_k(x_i,y_j)^2 \\ &\text{subject to} && 0 \leqslant v_i \leqslant v_{\max}, \quad i = 0,1,\ldots,N \\ & && \|\boldsymbol{a}(t)\| \leqslant a_{\max}, \quad t \in [0,T] \end{aligned} \tag{5}$$

$\boldsymbol{a}(t) = [a_x(t), a_y(t)]^T$ is the nozzle acceleration. $v_{\max}$ and $a_{\max}$ are the maximal speed and acceleration permissible for the AM hardware or the process, respectively. $e_k : \mathbb{R}^2 \to \mathbb{R}$ is an error function that measures the deviation of the actual (given the speeds V) height w.r.t. the goal height. We consider two error functions:

1. Direct comparison between the actual and the goal height:
$$e_1(\mathbf{x}) = \left|H(\mathbf{x}) - H_G^\theta(\mathbf{x})\right| \tag{6}$$
2. A more permissive function to diminish underfill due to nozzle acceleration:
$$e_2(\mathbf{x}) = \begin{cases} \left|H(\mathbf{x}) - H_G^\theta(\mathbf{x})\right|, & H(\mathbf{x}) < H_G^\theta(\mathbf{x}), \text{i.e. underfill} \\ 0, & H_G^\theta(\mathbf{x}) \leqslant H(\mathbf{x}) \leqslant \max(H_G^\theta), \\ & \text{i.e. permissible overfill} \\ H(\mathbf{x}) - \max(H_G^\theta), & H(\mathbf{x}) > \max(H_G^\theta), \text{i.e. overfill} \end{cases} \tag{7}$$

where $\max(H_G^\theta) = H_0(x, 0) = \frac{\sqrt{2}f}{\rho\sqrt{\pi R v}}$.

4. Results

For the purpose of illustration, we produce the results of minimizing over-deposition with corner angles $\theta \in \{30^\circ, 60^\circ, 90^\circ\}$ and use the conditions of Table 1. The material properties specific for LMD used in the simulation correspond to *AISI 316L* stainless steel in [22].

Table 1
Simulation set-up. Parameters for the optimization of material overfill at the corners deposition. Values based on Refs. [20,22,23].

Parameter	Value
Material	*AISI 316L*
Density	$\rho = 7900$ kg/m^3 [23]
Clad radius	$R = 2.3$ mm
Nozzle cruising speed	$v_c = 13$ mm/s
Material feed rate	$f = 0.42$ g/s
Maximal speed	$v_{\max} = 2v_c = 26$ mm/s
Maximal acceleration	$a_{\max} = 600$ mm/s^2 [20]

Our model parametrizes the magnitude of the dispenser cruise speed in terms of the distance d from the corner tip. We approximate the optimal speed function V^O by a 4-stage PL function (see Table 2). The stages of V^O are nonlinear functions of d. Given consecutive checkpoints (d_i, v_i) and (d_{i+1}, v_{i+1}) the velocity between them is given by:

$$V^O(d) = \sqrt{2a(d - d_i) + v_i^2}, \quad d \in [d_i, d_{i+1}], \tag{8}$$

where a is the constant acceleration in the stage.

The minimization uses the exhaustive search method to find the optimal velocity histories for error accountancy methods e_1 and e_2. This method is expensive in computing time. Therefore, this

Table 2
Row 1: Optimal speed profiles $V^O_{e_1}, V^O_{e_2}$ for errors e_1 and e_2. Corner angles $\theta \in \{30^\circ, 60^\circ, 90^\circ\}$. Rows 2–6: Resulting bead geometries. Row 2: no velocity control. Rows 3–4: Beads with optimal velocity, given errors e_1 and e_2, respectively. Rows 5–6: Bead cross-section $Y = 0$ with optimal velocity, given errors e_1 and e_2, respectively.

	$\theta = 30^\circ$	$\theta = 60^\circ$	$\theta = 90^\circ$
Optimal speed histories. Errors e_1 and e_2	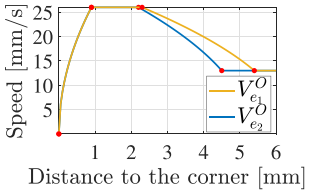	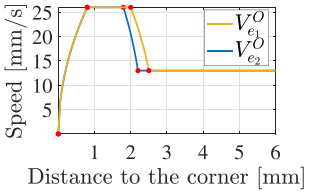	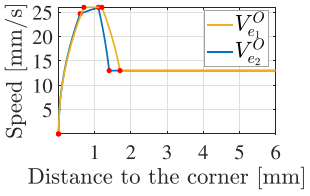
Bead geometry for constant velocity V_{v_c}	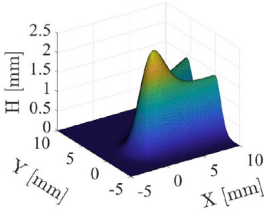	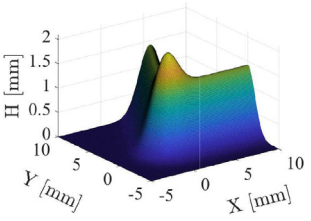	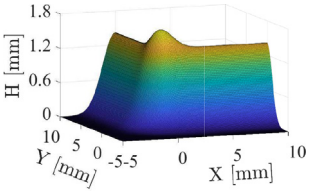
Optimized bead geometry. Optimal velocity $V^O_{e_1}$	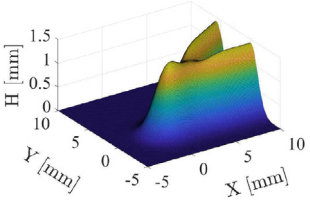	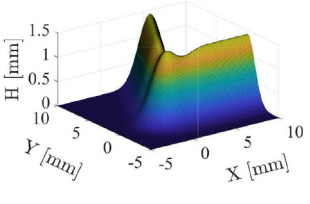	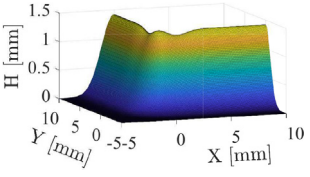
Optimized bead geometry. Optimal velocity $V^O_{e_2}$	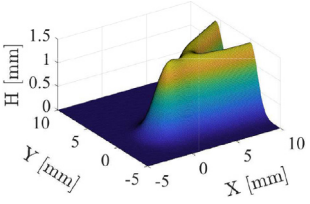	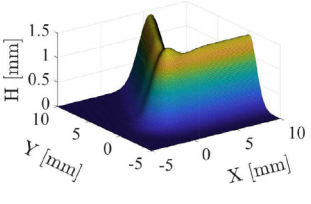	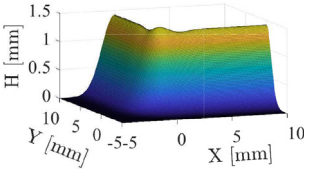
Optimized bead cross-section $Y = 0$. Optimal velocity $V^O_{e_1}$	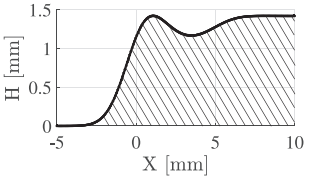	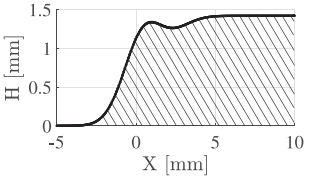	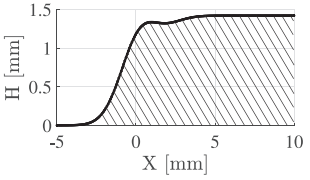
Optimized bead cross-section $Y = 0$. Optimal velocity $V^O_{e_2}$	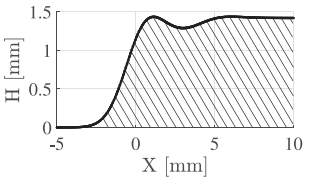	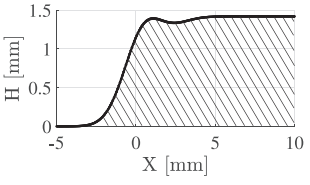	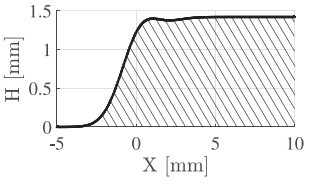

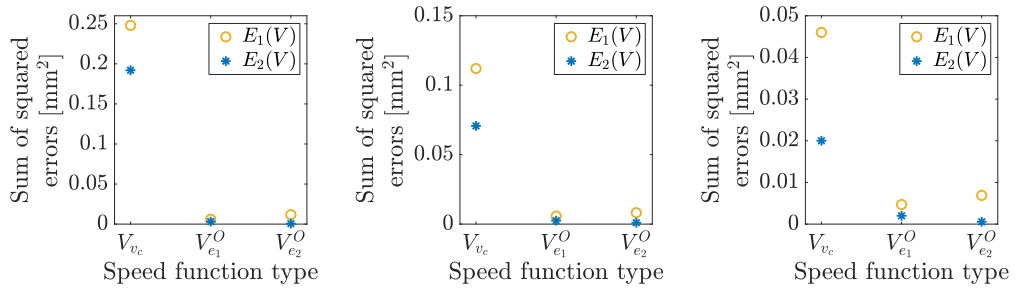

(a) Corner angle $\theta = 30°$. (b) Corner angle $\theta = 60°$. (c) Corner angle $\theta = 90°$.

Fig. 2. Over-deposition consolidated estimators E_1 and E_2 (Eq. (5)) for velocity profiles $\{V_{v_c}, V^O_{e_1}, V^O_{e_2}\}$ and corner angles $\{30°, 60°, 90°\}$. e_1 and e_2: deposition punctual error methods (Eqs. (6) and (7), respectively).

optimization is to be used at the stage of process-planning and not in real time during the manufacturing itself. The resulting speed profiles for each studied value of the corner angle θ are presented in Table 2. For each angle, we found speed profiles $V^O_{e_1}$ and $V^O_{e_2}$ as per the error e_1 and e_2 functions in Eqs. (6) and (7).

The (decreasing) distance to the next corner presents velocity plots which occur in the negative horizontal axis. However, notice that the entry and exit velocity histories are, under the current assumptions, symmetrical with respect to the distance to the corner spot. These considerations lead to Table 2 presenting the dispenser velocity at the *exit* from the corner and not in the *entry* phase. Both, $V^O_{e_1}$ and $V^O_{e_2}$ show similar behavior: (a) large acceleration near the corner, reaching the maximal value $v_{\max}$, (b) constant speed, and (c) deceleration to reach the cruise speed v_c. The sharper the corner, the smaller the angle θ and (as expected) the more abrupt the acceleration or deceleration near the corner spot. Error accountancy methods e_1 and e_2 call for the same acceleration (or deceleration) to depart from (or reach to) null velocity at the corner. However, the transition to cruise speed takes longer with method e_1. Therefore, the average speed of $V^O_{e_1}$ is greater than the one of $V^O_{e_2}$.

Table 2 shows the height functions for $\theta \in \{30°, 60°, 90°\}$ associated to (1) the optimal speed functions $V^O_{e_i}$ $(i = 1, 2)$ and (2) a simulation with a constant speed function V_{v_c} (which would require infinite acceleration/deceleration at the corner spot).

In Table 2, (1) we can observe the material over-deposition at constant speed V_{v_c} is evident for all $\theta \in \{30°, 60°, 90°\}$. Additionally, over-deposition increases when the angle decreases. (2) In the cross-section views for $\theta = 30°$, we can note that $V^O_{e_1}$ produces more underfill than $V^O_{e_2}$. Since the average speed of $V^O_{e_1}$ is greater than the one of $V^O_{e_2}$, the amount of deposited material is lower.

The values of the objective functions (i.e. sum of squared errors in Eq. (5)) for the optimal velocity functions $V^O_{e_1}$ and $V^O_{e_2}$, and for the constant (uncontrolled) velocity function V_{v_c} are depicted in Fig. 2. The difference of the objective functions between the optimal $(V^O_{e_1}, V^O_{e_2})$ and uncontrolled (V_{v_c}) velocity functions is noticeable. The values under uncontrolled speed are at least 10 times greater than for the optimal solutions $(E_i(V_{v_c})/E_i(V^O_{e_i}) > 10, i = 1, 2)$. We can also observe that, for every value of $\theta \in \{30°, 60°, 90°\}$, the minimal value of E_1 is attained by $V^O_{e_1}$ (analogously for E_2 and $V^O_{e_2}$).

5. Conclusions

In this manuscript, we have presented the implementation of a voxel-based geometric simulator for Laser Metal Deposition (LMD). On this simulator, we have mounted and solved a minimization of the material over-deposition at corners in LMD. Results for the corner angle instances $\theta \in \{30°, 60°, 90°\}$ show a reduction of over 90% of the over-deposition present at corners with no nozzle velocity control. An *exhaustive search* strategy is used for minimization. This strategy is expensive in computing time. Therefore, our method is to be used for the process planning stage. Further study of heuristics for cutting computing time expenditures are required for in-process applications.

Funding

This work has been partially funded by the Basque Government under ELKARTEK program (grants KK-2018/00115 (ADDISEND) and KK-2019/00006 (B4H)), and by the INZU Group (Talens Systems and Ikergune A.I.E.).

Declaration of Competing Interest

The authors declare that they have no known competing financial interests or personal relationships that could have appeared to influence the work reported in this paper.

References

[1] Leino M, Pekkarinen J, Soukka R. The role of laser additive manufacturing methods of metals in repair, refurbishment and remanufacturing – enabling circular economy. Phys Proc 2016;83:752–60.
[2] Montoya-Zapata D, Creus C, Ortiz I, Alvarez P, Moreno A, Posada J, et al, Generation of 2.5d deposition strategies for lmd-based additive manufacturing. Proc Comput Sci 2021:180;280–289. Proceedings of the 2nd international conference on industry 4.0 and smart manufacturing (ISM 2020).
[3] Woo Y, Han S, Oh I, Moon Y, Ha W. Control of directed energy deposition process to obtain equal-height rectangular corner. Int J Precis Eng Manuf 2019;20(12):2129–39.
[4] Giberti H, Sbaglia L, Urgo M. A path planning algorithm for industrial processes under velocity constraints with an application to additive manufacturing. J Manuf Syst 2017;43:160–7.
[5] Ertay DS, Yuen A, Altintas Y. Synchronized material deposition rate control with path velocity on fused filament fabrication machines. Addit Manuf 2018;19:205–13.
[6] Pereira JC, Borovkov H, Zubiri F, Guerra MC, Caminos J. Optimization of thin walls with sharp corners in SS316L and IN718 alloys manufactured with laser metal deposition. J Manuf Mater Process 2021;5(1):5.
[7] Comminal R, Serdeczny MP, Pedersen DB, Spangenberg J. Numerical modeling of the material deposition and contouring precision in fused deposition modeling. In: Proceedings of the 29th Annual International Solid Freeform Fabrication Symposium 2018: An Additive Manufacturing Conference. Laboratory for Freeform Fabrication; 2018. p. 1855–64.
[8] Comminal R, Serdeczny MP, Pedersen DB, Spangenberg J. Motion planning and numerical simulation of material deposition at corners in extrusion additive manufacturing. Addit Manuf 2019;29:100753.
[9] Caiazzo F, Alfieri V. Simulation of laser-assisted directed energy deposition of Aluminum powder: Prediction of geometry and temperature evolution. Materials 2019;12(13):2100.

[10] El Cheikh H, Courant B, Branchu S, Hascoët J-Y, Guillén R. Analysis and prediction of single laser tracks geometrical characteristics in coaxial laser cladding process. Opt Lasers Eng 2012;50(3):413–22.
[11] Ocelík V, Nenadl O, Palavra A, De Hosson J. On the geometry of coating layers formed by overlap. Surf Coat Technol 2014;242:54–61.
[12] Nenadl O, Ocelík V, Palavra A, De Hosson JT. The prediction of coating geometry from main processing parameters in laser cladding. Phys Proc 2014:56;220–227. 8th international conference on laser assisted net shape engineering LANE 2014.
[13] Zhou S, Dai X, Zheng H. Analytical modeling and experimental investigation of laser induction hybrid rapid cladding for Ni-based WC composite coatings. Opt Laser Techol 2011;43(3):613–21.
[14] Ya W, Pathiraj B, Liu S. 2D modelling of clad geometry and resulting thermal cycles during laser cladding. J Mater Process Technol 2016;230:217–32.
[15] Tian H, Chen X, Yan Z, Zhi X, Yang Q, Yuan Z, Finite-element simulation of melt pool geometry and dilution ratio during laser cladding. Appl Phys A 2019:125 (7).
[16] Lalas C, Tsirbas K, Salonitis K, Chryssolouris G. An analytical model of the laser clad geometry. Int J Adv Manuf Technol 2006;32(1–2):34–41.
[17] Arrizubieta JI, Lamikiz A, Klocke F, Martínez S, Arntz K, Ukar E. Evaluation of the relevance of melt pool dynamics in laser material deposition process modeling. Int J Heat Mass Transf 2017;115:80–91.
[18] Tabernero I, Lamikiz A, Ukar E, López de Lacalle L, Angulo C, Urbikain G. Numerical simulation and experimental validation of powder flux distribution in coaxial laser cladding. J Mater Process Technol 2010;210(15):2125–34.
[19] Tabernero I, Lamikiz A, Ukar E, Martínez S, Celaya A. Modeling of the geometry built-up by coaxial laser material deposition process. Int J Adv Manuf Technol 2013;70(5):843–51.
[20] Arrizubieta JI, Martínez S, Lamikiz A, Ukar E, Arntz K, Klocke F. Instantaneous powder flux regulation system for laser metal deposition. J Manuf Processes 2017;29:242–51.
[21] Ding Y, Warton J, Kovacevic R. Development of sensing and control system for robotized laser-based direct metal addition system. Addit Manuf 2016;10:24–35.
[22] Alvarez P, Montealegre MA, Pulido-Jiménez JF, Arrizubieta JI. Analysis of the process parameter influence in laser cladding of 316L stainless steel. J Manuf Mater Process 2018;2(3):55.
[23] Pichler P, Simonds BJ, Sowards JW, Pottlacher G. Measurements of thermophysical properties of solid and liquid NIST SRM 316L stainless steel. J Mater Sci Dec 2019;55:4081–93.